METAL–SEMICONDUCTOR TRANSITIONS IN NANOSCALE VANADIUM DIOXIDE—THIN FILMS, SUBWAVELENGTH HOLES, AND NANOPARTICLES

By

Eugenii U. Donev

Dissertation

Submitted to the Faculty of the

Graduate School of Vanderbilt University

in partial fulfillment of the requirements

for the degree of

DOCTOR OF PHILOSOPHY

in

Physics

December 2008

Nashville, Tennessee

Approved:

Leonard C. Feldman

Richard F. Haglund, Jr.

Deyu Li

James H. Dickerson

Sharon M. Weiss

CHAPTER VI

SIZE-EFFECTS IN THE STRUCTURAL PHASE TRANSITION OF VO_2 NANOPARTICLE ARRAYS STUDIED BY SURFACE-ENHANCED RAMAN SCATTERING

Abstract

Described here is the first experimental application of surface-enhanced Raman scattering (SERS) to the study of the phase transition of vanadium dioxide (VO_2). Using arrays of hybrid gold-capped VO_2 nanoparticles (Au+VO_2 NPs) and a VO_2 film covered with Au islands, we obtained the temperature evolution of the SERS intensity with respect to the amount of accessible VO_2 material across the monoclinic-tetragonal-monoclinic transformation cycle. Overall, we found that the smallest Au+VO_2 NPs required the largest deviations from the bulk transition temperature to complete their phase transition, resulting in the widest thermal hysteresis, while the Au+VO_2 film exhibited the narrowest hysteresis. Although the observed size-dependence agreed with the model of defect-induced nucleation of the VO_2 phase transition, the observed magnitude and change of the hysteresis width with NP size were less pronounced than those in a previous study of elastic light scattering from arrays of bare VO_2 NPs. The discrepancies likely stem from the creation of extrinsic defect sites in the VO_2 material owing to the presence of Au during the high-temperature processing. Finally, we correlated the size-dependence of the measured VO_2 SERS intensity with the scattering efficiency of the Au particles, within the framework of a modified Mie-theory calculation.

6.1 Introduction

6.1.1 Motivation

The present work is an extension of the Raman study of *single* VO_2 NPs presented in Chapter V. Briefly, VO_2 undergoes a temperature-driven metal-semiconductor transition at $T_c \approx 340$ K, which causes profound changes not only in the electronic configuration but also in the crystallographic structure of the material, which switches from a monoclinic (semiconductor) phase (below T_c) to a tetragonal/rutile (metal) phase.[22,23] The single-NP Raman study demonstrated the feasibility of measuring a well-known signature of the structural transition of VO_2—the disappearance of certain Raman-active vibrational modes—but in isolated, nanoscale amounts of VO_2. The potential value of such single-NP measurements exceeds the mere "proof of concept" because they provide a practicable method for gathering particle-by-particle statistics on the "potent" defect sites deemed responsible for nucleating the VO_2 phase transition. As an intermediate step along this route, we set out to investigate the size-dependent properties of *arrays* of VO_2 NPs across their temperature-driven structural transformation.

The interest in size-effects in the VO_2 phase transition is relatively new. Lopez *et al.*[9] studied ordered arrays of VO_2 NPs by incoherent elastic light scattering, and reported size-dependent transition temperatures, as well as an intrinsic variability in the transition temperatures of nominally identical NPs within the same array, which gives rise to intermediate states of increased scattering. Such states of maximum scattered intensity, indicated as points "C" and "G" in Figure 6.1b, arise under conditions of maximum disorder when about half of the NPs in an array have switched from semiconducting to metallic (point "C"), or *vice versa* (point "G"). Regarding the size-dependence of T_c during heating and cooling, the authors found that the hysteresis loops widen as the NP diameters decrease (Figure 6.1c), in qualitative agreement with the model of defect-initiated nucleation of the VO_2 phase transition[5] (see also Section 1.3.2). In view of the still-debated issue of the relative roles of lattice distortion and electron-electron correlations in the mechanism of

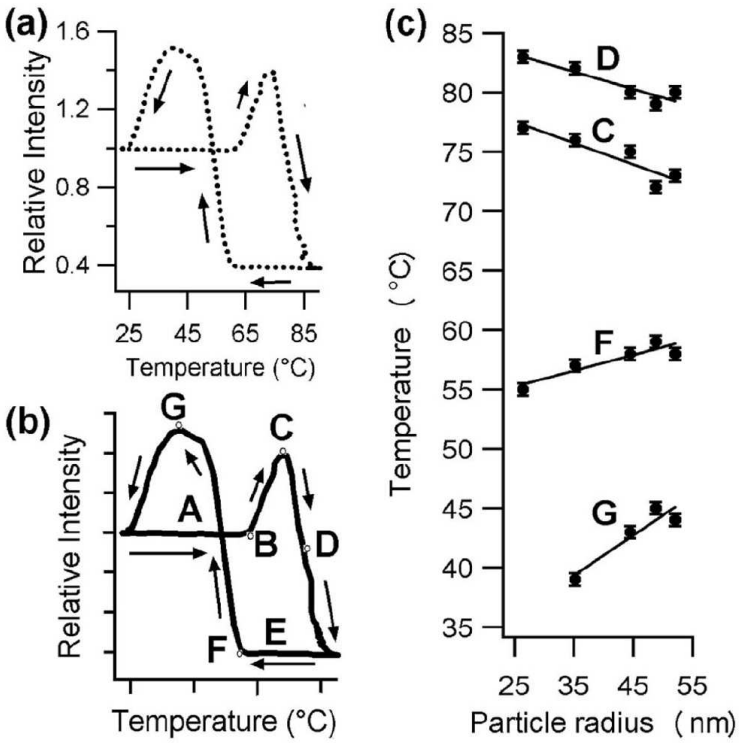

Figure 6.1: **(a)** Temperature evolution of incoherent light scattering at $\lambda = 600$ nm from array of VO_2 NPs. **(b)** Typical hysteresis loop of scattered light from one such array, with indicator points along VO_2 semiconductor-metal-semiconductor phase transition. **(c)** Temperatures of indicator points during a cycle of the VO_2 phase transition as a function of NP size (solid lines are only meant to guide the eye). After Lopez *et al.*[9]

the VO_2 phase transition[1–3,25–32] (see also Section 1.1.3), and because Lopez *et al.*'s light-scattering study[9] probed mainly the electronic response of VO_2 NPs, it is fair to say that the work presented here was partly motivated by curiosity to discover whether probing solely the structural transition of VO_2 NPs (through Raman-active phonon modes) would yield a different size-dependence and possibly shed light on the nature, electronic *vs.* structural, of the elusive "nucleating defects". We shall return to Figure 6.1c in Section 6.3.2.

6.1.2 SERS from hybrid Au+VO_2 NPs

Unfortunately, we were unable to detect any usable Raman signal from arrays of bare-VO_2 NPs of interesting sizes (*i.e.*, diameters of about 100 nm and smaller). A scanning

electron micrograph (SEM) of one such array on a silicon (Si) substrate is shown in Figure 6.2a, and its Raman spectrum in Figure 6.2b. Despite the very long integration time (60 minutes) and relatively large average NP size (110 nm), only Raman peaks belonging to the Si substrate stand out distinctly above the background level. The weak spectral feature just below 200 cm^{-1}, while indeed attributable to the 195-cm^{-1} mode of VO_2, was indistinguishable from noise in the spectra of arrays of smaller VO_2 NPs. In fact, it was not until 125-nm NPs were measured (not shown) that clear, though still weak, VO_2 Raman peaks emerged.

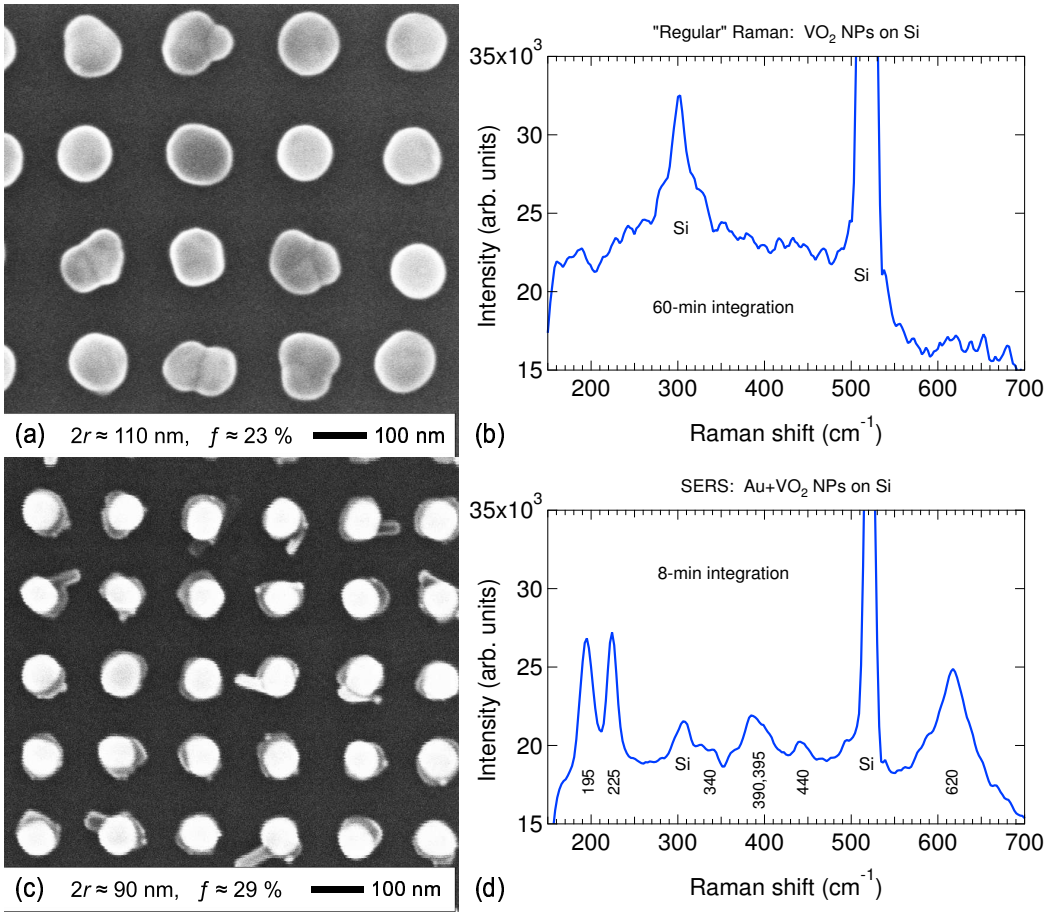

Figure 6.2: Scanning electron micrographs (SEMs) ($2r \equiv VO_2$ NP diameter; $f \equiv$ areal coverage) and room-temperature Raman spectra from arrays of **(a, b)** bare and **(c, d)** Au-capped VO_2 NPs on Si. Note the presence of several strong VO_2 peaks in the Au+VO_2 case, owing to signal enhancement (SERS effect) from the Au caps despite the shorter collection time (8 *vs.* 60 min) and smaller NP sizes (90 *vs.* 110 nm).

Raman scattering is inherently an extremely weak process, with cross-sections per molecule ($\sim 10^{-30}$ cm^2) that are typically 14–15 orders of magnitude smaller than fluorescence cross-sections.[112] In comparison with Raman scattering from bulk materials, thin films, or large particles, the situation becomes progressively less favorable for smaller and smaller NPs, since the reduced volume and elastic scattering efficiency of the latter weaken the interaction with the excitation light even further. Fortunately, the electromagnetic field enhancement associated with the *collective* oscillations of the free electrons—the surface plasmons—of noble metals can be harnessed to greatly increase the interaction strength between an analyte and optical radiation. This notion finds its most prominent realization in the technique of surface-enhanced Raman scattering (SERS). In SERS, the analyte, which may even consist of single molecules, is placed in close proximity (a few nm) or in contact with the signal enhancer (usually made of Ag or Au), which can be a roughened metal substrate, granular metal film, colloidally dispersed or lithographically patterned metal NPs.

In the hope of overcoming the weakness of "regular" Raman scattering from VO_2 NPs, we fabricated hybrid Au+VO_2 nanostructures, as described below (Section 6.2), which consisted of VO_2 NPs "capped" with Au NPs (*e.g.*, see Figure 6.2c). The improvement in signal strength due to the SERS effect was spectacular: for example, the SERS spectrum in Figure 6.2d shows a number of intense VO_2 peaks, especially the two peaks of interest at 195 and 225 cm^{-1}, even though the VO_2 NPs in this array were smaller ($2r_{\mathrm{Au+VO2}} \approx 90$ nm *vs.* $2r_{\mathrm{onlyVO2}} \approx 110$ nm) and the integration time much shorter ($t_{\mathrm{Au+VO2}} = 8$ min *vs.* $t_{\mathrm{onlyVO2}} = 60$ min). Smaller (down to 50 nm) as well as larger (up to 150 nm) hybrid Au+VO_2 NPs also produced distinguishable VO_2 peaks, but invariably of lower intensity than the 90-nm Au+VO_2 NPs. To see why this was so, we recall that the main contribution to signal enhancement in SERS, the electromagnetic effect (as opposed to the "chemical" one), scales roughly with the fourth power of the electric-field enhancement because the Stokes shifts (*i.e.*, vibrational frequencies) of the analyte are usually small enough in comparison with the plasmon bandwidth of the metal, so that the local fields at both the excitation frequency

of the incident radiation and the Stokes frequency of the induced-dipole radiation become enhanced[112,113] (see also Section 2.6.3). Since both of these enhancement factors originate from the interaction of optical radiation with metal nanostructures, the *scattering efficiency* of a field enhancer plays a key role in determining the magnitude of signal enhancement obtainable from a SERS measurement.

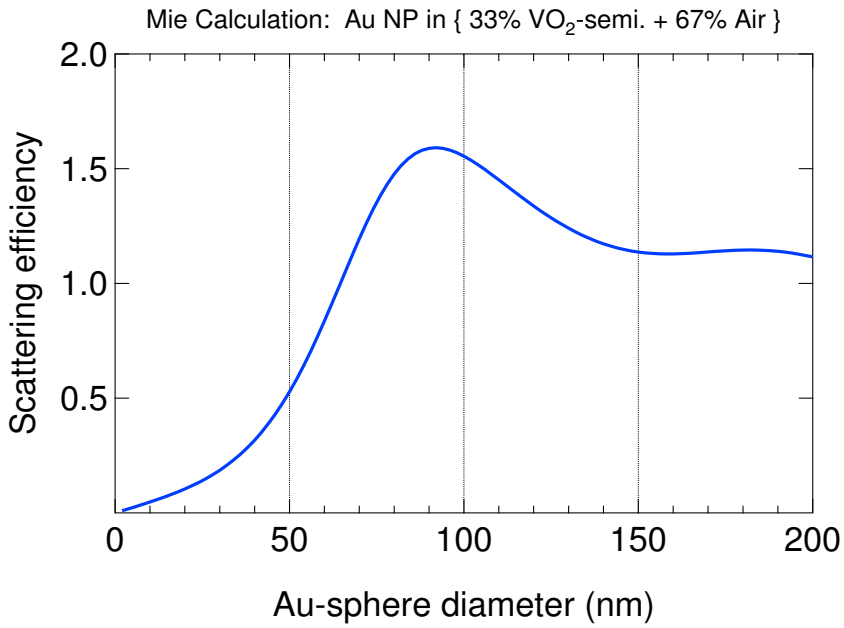

Figure 6.3: Mie-theory calculation (modified for absorbing host medium) of scattering efficiency as a function of particle diameter for Au sphere in composite host medium consisting of $\frac{1}{3}$ VO_2 (semiconducting phase) and $\frac{2}{3}$ Air. Note that the highest efficiency occurs at $2r_{Au} = 90$ nm, *apparently* (see Section 6.1.2) in accord with the largest measured SERS intensity (cf, Figures 6.9 and 6.10, right panels).

Figure 6.3 shows an analytical calculation, based on the Mie theory of light scattering[120] but modified to account for an absorbing host medium,[119] of the scattering efficiency as a function of size for a spherical Au particle immersed in a composite host medium. The complex permittivity of the host medium consists of weighted contributions of VO_2 and air; the permittivity of Au was obtained from Reference [184], and that of VO_2 from Reference

[57]. The specific choice of 33% VO_2 and 67% air was prompted by a simple geometrical argument: assuming a hemispherical Au "cap" on a flat VO_2 surface, $\frac{1}{3}$ of the cap's surface area lies in contact with VO_2 and $\frac{2}{3}$ with air. Despite using this *ad hoc* assumption in conjunction with a calculation for a sphere, Mie theory predicts the maximum scattering efficiency of such Au NPs to peak precisely at $2r_{\mathrm{Au}} = 90$ nm—apparently in excellent agreement with the strongest SERS signal measured in the present study (Figure 6.2d; see also Section 6.1.2 for a minor correction to this calculation).

6.2 Experimental details

Arrays of Au-capped VO_2 NPs, along with a Au-covered patch of VO_2 film, were fabricated on a Si substrate by means of: **(i)** electron-beam lithography (EBL: 30-kV accelerating voltage, 10-μm beam aperture, 40-pA beam current, 10-mm working distance, 1000 X magnification) in a spin-coated layer of poly(methyl-methacrylate) (PMMA: 100-nm thickness, 950K molecular weight), followed by chemical removal of the exposed areas; **(ii)** pulsed-laser deposition (PLD: KrF excimer laser at $\lambda = 248$ nm, fluence ≈ 3 J·cm^{-2}, V_2O_3 pressed-powder target, O_2 gas at 5 mtorr) of amorphous, sub-stoichiometric vanadium oxide ($VO_{1.7}$, 20-nm thickness); **(iii)** electron-beam evaporation of gold (Au: 15-nm thickness); **(iv)** chemical lift-off of the remaining PMMA and its Au+$VO_{1.7}$ overlayer; **(v)** thermal anneal (450 $^{\mathrm{o}}$C, O_2 gas at 250 mtorr, 30 min) of the resulting Au+$VO_{1.7}$ structures in order to render the VO_2 film patch and NPs stoichiometric and crystalline.[45] Nanoparticles of different sizes were obtained by either defining lithographic areas of given lateral dimensions (mainly for the larger NPs), or by varying the dwell time in "dot exposures"—that is, exposing the PMMA to a greater amount of electron charge in one spot to make a larger NP (*e.g.*, 10/29/48 fC per "dot" for NPs of 50/70/90-nm average diameters). According to the expected NP size, the lattice spacing of the NP arrays was also varied, between 75 and 250 nm, in order to keep the areal coverage approximately constant.

Scanning electron micrographs (SEMs) showing sections of the Au+VO_2 film patch

(Figure 6.8(a, b)) and Au+VO_2 NP arrays (Figures 6.9(a, c, e) and 6.10(a, c, e)) reveal that the Au layer does not wet the VO_2 layer very well, leading to the formation of Au islands on the film patch and "balled-up" Au caps on the VO_2 NPs; moreover, as particle size increases, the Au caps appear to cover less of the surface area of their underlying VO_2 NPs. Another feature peculiar to the morphology of these hybrid NPs, which was absent prior to the thermal anneal (step (v) above), is the finger-like protrusions that extend from some of the NPs or even bridge the gap between a pair of neighboring NPs, especially in arrays of smaller NP sizes and spacings. Judging solely from the contrast in the SEM images, most of the protrusions seem to consist of VO_2 without Au on top.

The arrays were excited using a continuous-wave laser light (He-Ne: $\lambda = 633$ nm, 45-mW output and 8-mW on-sample power), fed through a monomode fiber into an optical microscope operating in confocal-reflection mode, then focused onto the sample with a micro-objective (60 X, NA = 0.80, $1/e^2$ beam spot ≈ 0.5 μm). The scattered light from the Au+VO_2 NPs or film, and from the Si substrate, was collected by the same micro-objective (backscattering geometry), filtered to reduce the elastic-scattering component, and sent through a multimode fiber to a spectrometer equipped with a cooled charge-coupled-device (CCD) detector. The sample temperature was ramped and maintained (± 0.05 K) using a controller unit that supplied power to a resistive heater based on the feedback from a temperature sensor under the heating plate.

Raman measurements were performed at several fixed temperatures, during heating and cooling, as follows: **(1)** the array or film patch of interest was positioned into the laser beam spot using manual micrometers, and imaged onto a CCD camera under concurrent white-light illumination; **(2)** the positioning was further fine-tuned by digital adjustments to the sample stage until two designated sample features coincided with two fixed on-screen markers; **(3)** the focus was visually adjusted by vertical displacement of the microscope head; **(4)** an 8-min Raman spectrum was collected. The sample was then heated up or cooled down, and the measurement sequence repeated at the next temperature point. We

thus obtained the evolution of the Raman response across the structural phase transition of VO_2. Unlike the single-NP experiment (Chapter V), here we measured the collective response as a function of size from *arrays of Au-capped* VO_2 NPs, where the NPs within each array were nominally identical.

6.3 Results and discussion

6.3.1 Peak statistics: Film vs. 90-nm NPs

Let us first compare the Raman response of the VO_2 film covered with Au islands and the response of an array of Au-capped VO_2 NPs (90-nm average diameter). As in Chapter V, we concentrate mainly on the peaks near 195 cm^{-1} and 225 cm^{-1}, which correspond to characteristic vibrational modes of the monoclinic (low-temperature) structure of VO_2 and vanish upon transition into the tetragonal (high-temperature) phase.[195–197,201] These phonon modes play a crucial role in the structural transition of VO_2, since they are associated with the pairing and tilting motions of V–V dimers that map the monoclinic onto the tetragonal lattice configuration.[31]

For the Au+VO_2 film and array of 90-nm NPs, Figure 6.4 shows representative spectra of the two peaks taken at room temperature (monoclinic phase), together with least-squares fits through the data points. Lacking *a priori* reasons to attribute the spectral linewidths to homogeneous (Lorentzian) or inhomogeneous (Gaussian) broadening mechanisms, Gaussian peak profiles were chosen because they fit the data better (*i.e.*, lower chi-square values); in fact, using Voigt functions, which are convolutions of a Lorentzian and a Gaussian,[205] resulted in fits weighted almost entirely in favor of the Gaussian profiles. The overall fits also included polynomial baselines to account for the background signal in the collected spectra. The fit parameters for the two VO_2 peaks, along with the Si-substrate peak near 520 cm^{-1} (*e.g.*, see Figure 6.2d), were obtained at each measured temperature point (heating and cooling) for which the fitting algorithm was able to "autofind" a peak.

The temperature evolutions of the positions and widths of the three peaks (VO_2: 195

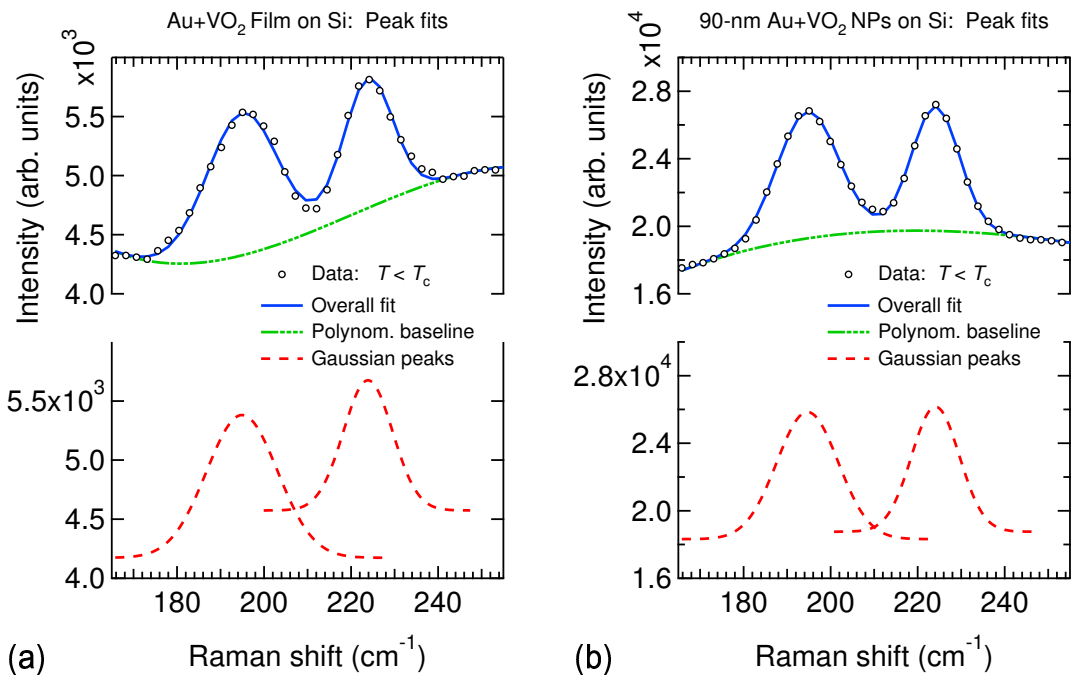

Figure 6.4: **(a)** Least-squares fits to VO_2 Raman peaks (two Gaussians + polynomial baseline) in the monoclinic phase of **(a)** Au+VO_2 film and **(b)** array of 90-nm Au+VO_2 NPs on Si.

cm^{-1} and 225 cm^{-1}; Si: 520 cm^{-1}) are presented in Figure 6.5. Regarding the spectral positions of the VO_2 peaks, a decrease in the Raman shift upon approaching the phase transition temperature—that is, lowering of the vibrational frequencies of the relevant phonon modes—would indicate a softening of the crystal lattice as it transforms from monoclinic to tetragonal. Despite the apparent involvement of the 195 and 225 cm^{-1} A_g-modes in the structural transformation,[31] only one Raman study[195] so far has claimed a spectral shift for either one of these peaks ($\pm$10 cm^{-1} at 195 cm^{-1}), although the authors did not specify whether the shift was positive (mode stiffening) or negative (mode softening). There have been observations[206,207] of a single soft mode at 149 cm^{-1} (up to -15 cm^{-1} shift between 300 K and T_c), while other workers[196,198] have observed no significant shifts of the monoclinic-VO_2 peaks. The data shown here (Figure 6.5(a, b)) suggest a slight softening of the 195-cm^{-1} mode of about 5 cm^{-1} towards higher temperatures (*i.e.*, closer to the tetragonal phase), whereas the positions of the 225-cm^{-1} peak remain unchanged within

the statistical uncertainties of the fits. Apart from those uncertainties, the estimated instrumental resolution of about ± 2 cm^{-1} renders the above -5 cm^{-1} shifts even less significant.

As for the spectral linewidths of the peaks (Figure 6.5(c, d)), the apparent narrowing near T_c, seen more clearly in the NP case, is likely an artifact of the fitting procedure, as automatic peak detection yields the least reliable "finds" right before a peak disappears entirely. Therefore, the highest-temperature fit points for each peak, both during heating and cooling, should be considered the most suspect. Without these, the NP peak widths change very little, while the large uncertainties in the case of the VO_2 film case make it hard to discern a trend. In both cases, however, the absolute width of the 195-cm^{-1} peak room-temperature exceeds that of the 225-cm^{-1}, in qualitative agreement with previously reported Raman spectra of VO_2 (*e.g.*, see Reference [195]).

The most interesting statistic extracted from the least-squares fits to the Raman data was the area under each peak as a function of temperature; the results are plotted in Figure 6.6. Three observations promptly stand out, and are discussed below.

First: In the NP case, the peak at 520 cm^{-1} due to the Si substrate exhibits hysteretic behavior instead of remaining oblivious to the phase transition in the VO_2 material. Furthermore, the Si hysteresis is "reversed" with respect to the VO_2 hysteresis—that is, the total intensity of the Si peak *increases* on heating through the monoclinic-to-tetragonal transition and *decreases* on cooling back into the monoclinic phase of the VO_2 NPs (cf, top panel *vs.* middle or bottom panels in Figure 6.6b). The cause of this behavior becomes clear once we consider the Raman response of tetragonal VO_2. Above T_c, symmetry constraints allow only four Raman-active vibrational modes,[207] which are also rather broad and heavily damped, likely because of interactions with the increased density of free carriers in metallic VO_2.[196] One of these modes results in a high-temperature VO_2 peak centered around 510 cm^{-1}—right underneath the Si-substrate peak at 520 cm^{-1}. As the VO_2 material transforms into the high-temperature phase, this tetragonal-phase mode grows and

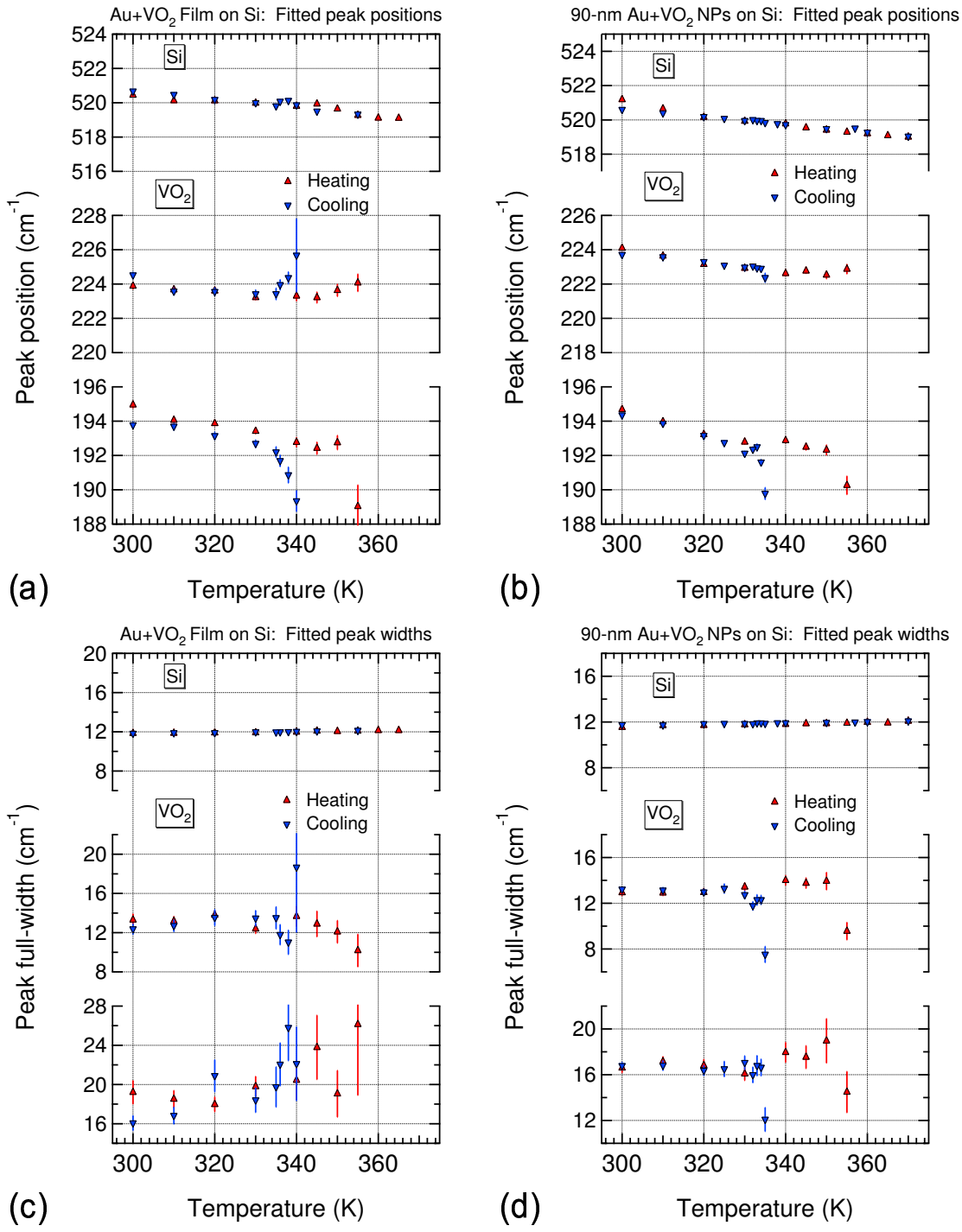

Figure 6.5: Peak statistics as a function of temperature (heating and cooling) for **(a, c)** Au+VO_2 film and **(b, d)** array of 90-nm NPs on Si, obtained from least-squares fits (see Figure 6.4) to the 195-cm^{-1} VO_2 peak (bottom panels), 225-cm^{-1} VO_2 peak (middle panels), and 520-cm^{-1} Si-substrate peak (top panels). For each peak: **(a, b)** full-width at half-maximum, **(c, d)** spectral position.

adds intensity to the Si peak; conversely, the disappearance of the mode towards the low-temperature phase diminishes the total intensity of the Si peak. Considering the different transition temperatures of VO_2 during heating and cooling, the Si peak also shows hysteretic behavior but in the reverse sense compared with the two monoclinic-VO_2 peaks. In the case of the Au+VO_2 film (Figure 6.6a), the temperature evolution of the Si-substrate peak does not seem to follow a clear trend, except near room temperature, where the lack of overlap between the heating and cooling data resembles the corresponding mismatch between the heating and cooling hysteresis branches of the two VO_2 peaks, possibly due to inconsistent focusing and/or power drift of the incident laser.

Second: The non-zero areas (total intensities) of the NP VO_2 peaks exceed their film counterparts by nearly an order of magnitude. Also, the film case lacks a conspicuous hysteresis loop for the Si peak, such as was seen in the NP case. These related observations can be attributed to the much weaker, if any, enhancement of the VO_2 Raman signal due to the Au islands of various shapes and sizes covering the film (Figure 6.8(a, b)), in contrast with the much greater enhancement from the Au NPs (Figure 6.10a)—on-resonance with the incident and scattered light (Figure 6.3). In other words, being critically reliant on size, shape, and surface morphology of the noble-metal structures to boost the *local* electromagnetic fields,[113] the SERS effect enhances the VO_2-NP peaks beyond their film counterparts, while scarcely influencing the signal from the more "remote" Si substrate (*i.e.*, spatially separated from the Au caps by the VO_2 layer).

Third: The NP array yielded VO_2 hysteresis loops that are clearly wider than those of the film patch. The dependence of the hysteresis width on NP size is further investigated in the next section.

6.3.2 Thermal hystereses: Size-dependence and comparison with previous results

With a view to uncovering a potential trend in the VO_2 structural transformation as a function of the amount of probed material, SERS spectra were measured from arrays of

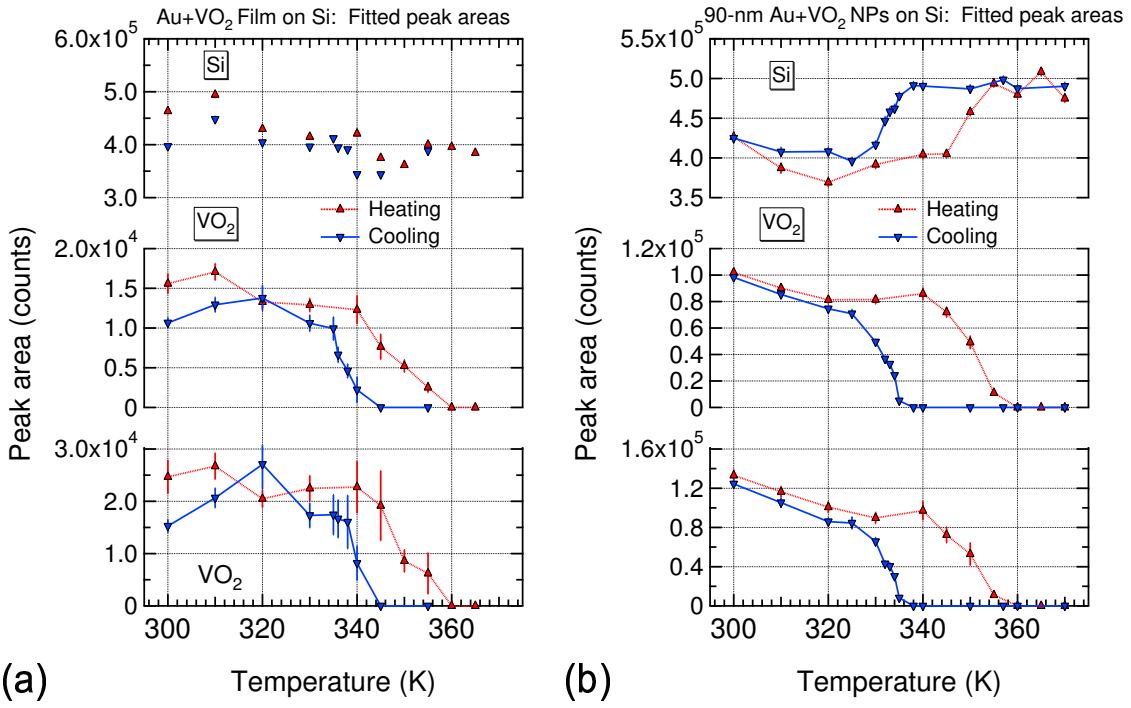

Figure 6.6: Integrated intensities (areas under Gaussian peaks in Figure 6.4) as a function of temperature (heating and cooling) for **(a)** Au+VO_2 film and **(b)** array of 90-nm NPs on Si, obtained from least-squares fits to the 195-cm^{-1} VO_2 peak (bottom panels), 225-cm^{-1} VO_2 peak (middle panels), and 520-cm^{-1} Si-substrate peak (top panels). All lines are only guides for the eye.

Au+VO_2 NPs of different sizes. Contrast analysis of SEM images, portions of which are shown in Figures 6.9(a, c, e) and 6.10(a, c, e), gave the following average diameters of the VO_2 NPs (but not necessarily of the corresponding Au caps): $2r \approx$ 50, 60, 70, 90, 130, 150 nm. For each of the six NP arrays and two spots on the film patch, Raman spectra were collected, as described above (Section 6.2), at ten or so temperature points during heating and about as many during cooling through the VO_2 phase transition. Figure 6.7 examines the region of interest from four such spectra out of the data sets for the smallest and largest NPs, below (300 K) and above (365 K) their transition temperatures upon heating. Once again, the vanishing of the peaks at 195 and 225 cm^{-1} marks the transition from monoclinic to tetragonal VO_2, and *vice versa*. As already noted in Chapter V, the 305-cm^{-1} Si peak decreases in intensity above the VO_2 phase transition owing to the vanishing of

an underlying VO_2 peak around 310 cm^{-1}. The background contribution was removed using an algorithm implementing a rolling-circle spectral filter, which distinguishes between peaks and baselines according to their radii of curvature.[202] Even after background subtraction, however, some intensity would often remain above the calculated baselines within the region of interest (175−245 cm^{-1}), whether due to random noise of small radius of curvature or to spectral features of the Si substrate, such as the one shown near 245 cm^{-1} in Figure 6.7a (top panel). It is because of this remanent intensity that the cumulative counts of the VO_2 peaks differ from zero even at the highest temperature points, well above T_c (*e.g.*, see the bases of the hysteresis loops in Figure 6.9).

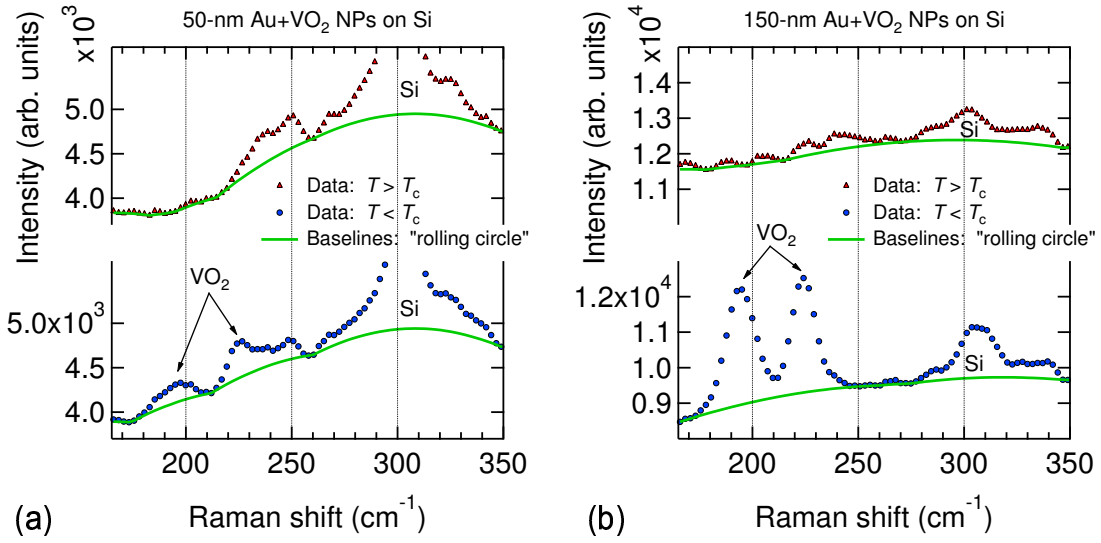

Figure 6.7: Representative SERS spectra from arrays of **(a)** 50-nm and **(b)** 150-nm Au+VO_2 NPs on Si, below and above their respective VO_2 transition temperatures. The solid lines denote the background levels calculated using a "rolling-circle" filter algorithm. The room-temperature (monoclinic) VO_2 peaks vanish in the high-temperature (tetragonal) phase, while features due to the Si substrate remain.

Thermal hystereses of the total above-baseline intensity between 175 and 245 cm^{-1} are presented in Figure 6.8c for one of the film spots; in Figure 6.9(b, d, f) for the 50, 60, 70-nm NPs; and in Figure 6.10(b, d, f) for the 90, 130, 150-nm NPs. The error bar of each

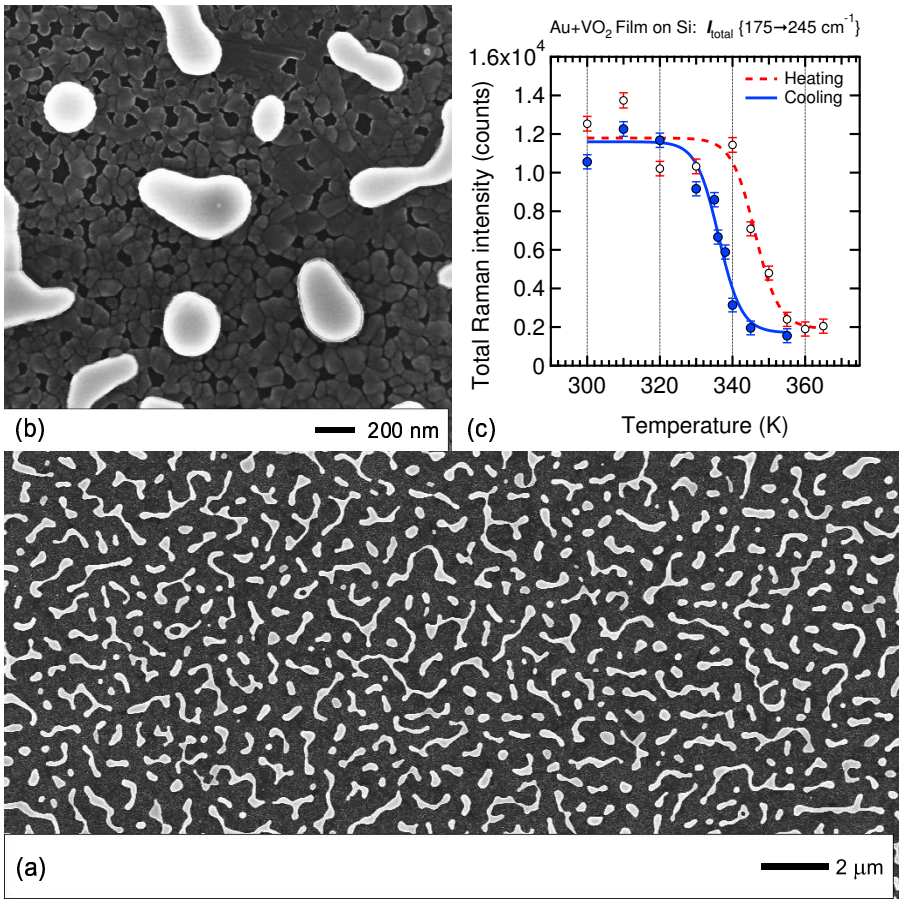

Figure 6.8: **(a, b)** SEM images of Au islands on VO_2 film on Si substrate, and **(c)** thermal hysteresis of SERS intensity of VO_2 peaks, summed between 175 and 245 cm^{-1} after "rolling-circle" background subtraction (see Figure 6.7). The lines are fits to the data points using an empirical sigmoidal function (see Equation 5.1).

data point denotes the uncertainty in determining the total intensity according to counting statistics: $I_{\text{total}} \pm \sqrt{I_{\text{total}}}$. Consequently, the significantly greater *relative* uncertainties for the smallest NP sizes (see Figure 6.9(b, d)) stem from their weaker (that is, less enhanced) Raman signals, as compared to the larger NPs (cf, VO_2 peaks in Figure 6.7a and 6.7b, bottom panels). The lines through the hysteresis data resulted from least-squares fitting with an empirical function of sigmoidal shape (see Equation 5.1), under the added constraint that the low- and high-temperature plateaus (I_{max} and I_{base}) of the heating and cooling branches overlap within the uncertainty of the fit. The main purpose of the fitting procedure was to provide a consistent measure of the transition temperatures for each hysteresis loop,

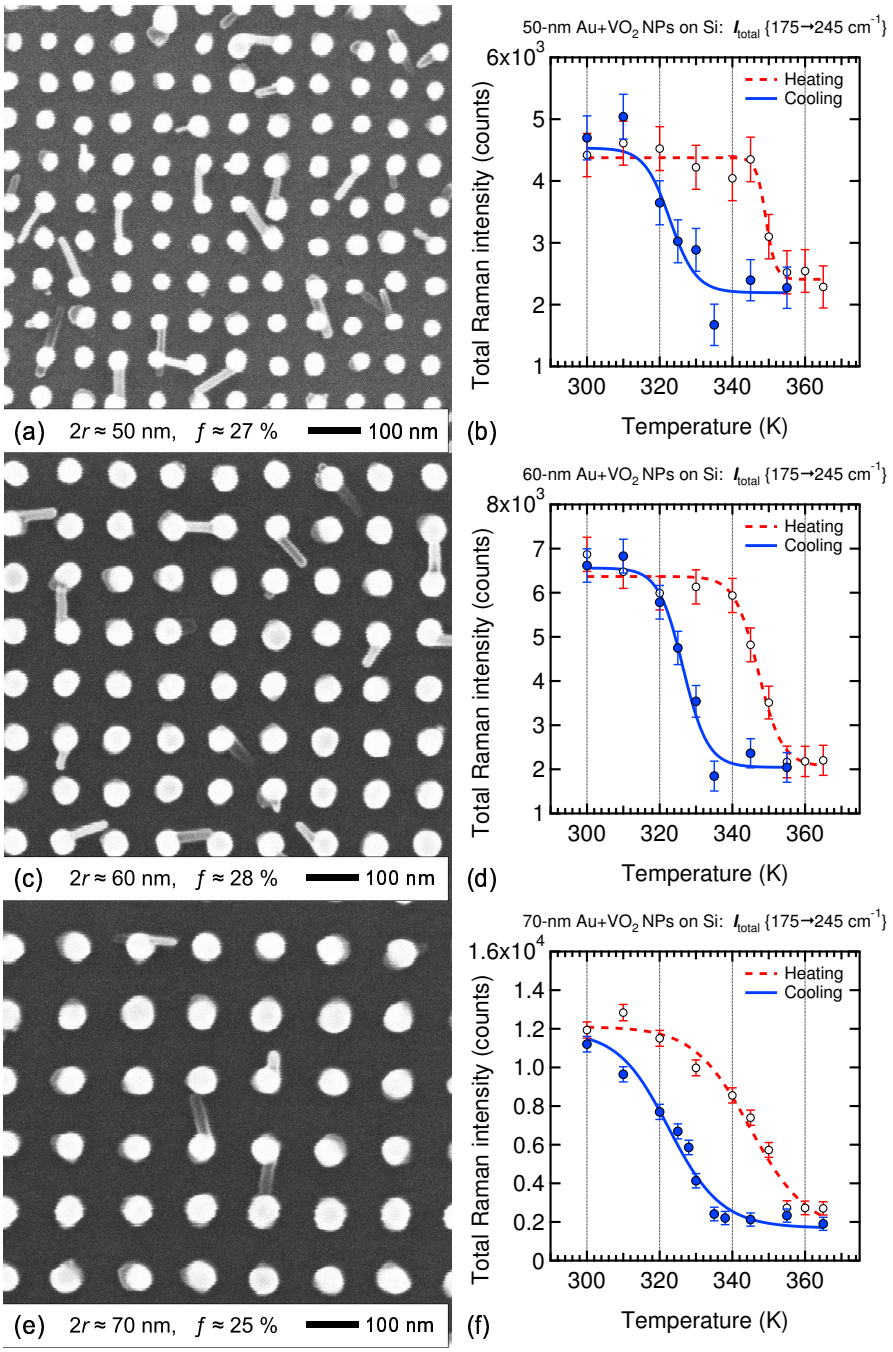

Figure 6.9: SEM images of arrays of Au-capped VO_2 NPs ($2r \equiv VO_2$ NP diameter; $f \equiv$ areal coverage), and thermal hystereses of SERS intensity of VO_2 peaks, summed between 175 and 245 cm^{-1} after "rolling-circle" background subtraction (see Figure 6.7), for $2r$ of **(a, b)** 50 nm, **(c, d)** 60 nm, and **(e, f)** 70 nm. The lines are fits to the data points using an empirical sigmoidal function (see Equation 5.1).

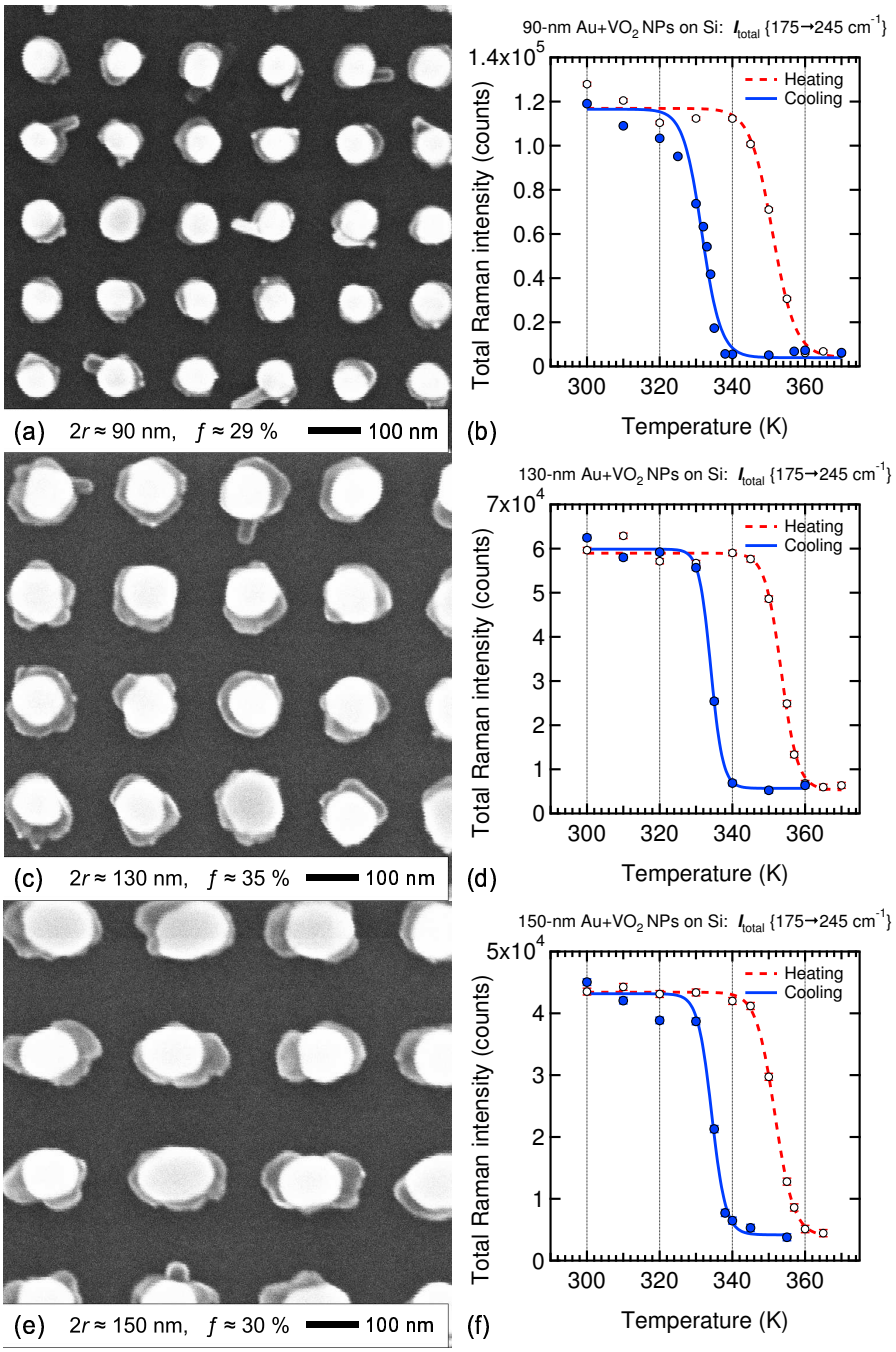

Figure 6.10: SEM images of arrays of Au-capped VO_2 NPs ($2r \equiv VO_2$ NP diameter; $f \equiv$ areal coverage), and thermal hystereses of SERS intensity of VO_2 peaks, summed between 175 and 245 cm^{-1} after "rolling-circle" background subtraction (see Figure 6.7), for $2r$ of **(a, b)** 90 nm, **(c, d)** 130 nm, and **(e, f)** 150 nm. The lines are fits to the data points using an empirical sigmoidal function (see Equation 5.1).

taken here as the half-maximum points (T_{half} in Equation 5.1) on the corresponding heating and cooling curves. Figure 6.11a summarizes those results for all six NP sizes and two separate spots on the film patch; the error bars here equal $\pm 1\sigma$, as calculated by the fitting routine.

Taking the film as a reference, we can now look for size-dependent trends in the NP data. For instance, most of the NP transition temperatures of the heating branch lie above the T_{c} of either film spot. Assuming that the total Raman intensity of the two VO_2 peaks is directly proportional to the overall amount of monoclinic-phase material, this means that, for example, half of the 130-nm VO_2 NPs would switch from monoclinic to tetragonal at a 7 ± 1 degrees higher temperature than half of the VO_2 material in the film. On the cooling branch, all the NP points lie below the corresponding T_{c} of the film; furthermore, the relative undercooling for the three smallest NP sizes is much more pronounced than their relative overheating. Large undercooling with respect to bulk T_{c}, previously observed in the aforementioned studies of VO_2 NPs implanted into silica[5] (Section 1.3.2) and arrays of VO_2 NPs on Si[9] (Figure 6.1), likely arises from asymmetric shear stress[5] present on transforming from the tetragonal (high-symmetry) back into the monoclinic (low-symmetry) phase, although a quantitative atomic-scale explanation is lacking. The cooling curve in Figure 6.11a then suggests that, for example, half of the 50-nm VO_2 NPs would return to the monoclinic phase at a 13 ± 2 degrees lower temperature than half of the film volume. In VO_2 nanocrystals, such thermal "delays" in switching phases are particularly pronounced because the availability of potent nucleation defects diminishes for smaller transforming volumes of VO_2, so that greater deviations from bulk T_{c} are required to drive the phase transition (see Chapter V, Section 5.3.2).

Before continuing, we ought to consider the possibility of plasmonic heating of the VO_2 NPs by means of light-energy dissipation in the Au caps. For example, Au NPs embedded in ice have been shown to generate localized heat and even melt the surrounding matrix under optical illumination, especially with a photon energy close to the particle-

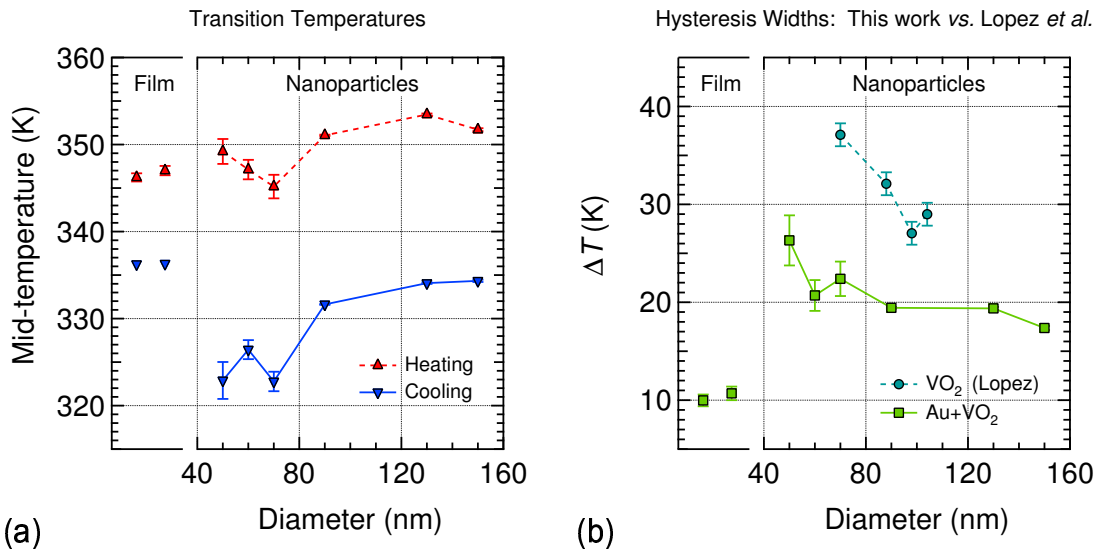

Figure 6.11: **(a)** Transition half-maximum points of heating and cooling branches of SERS hystereses (obtained from sigmoidal fits in Figures 6.8, 6.9, 6.10) for two different spots on the Au+VO_2 film (left panel) and for all six NP sizes (right panel). **(b)** Comparison between hysteresis widths from SERS measurements on Au+VO_2 film (left panel) and NPs (right panel) on Si (this work) and hysteresis widths from light-scattering measurements on VO_2 NPs on Si (after Lopez *et al.*,[9] see Figure 6.1 and text). All lines are only meant to guide the eye.

plasmon resonance.[208] Theoretical analysis of the mechanism of heat generation in a Au NP reveals that the maximum increase in local temperature due to plasmonic heating occurs at the surface of the particle and scales with the square of its radius.[208,209] It is then conceivable that the VO_2 transition temperatures obtained in this study may have been biased by an additional source of heat besides the sample heater. Such an effect would manifest itself as an "artificial" decrease in the observed T_c *in either direction*, since less external energy (as registered by the temperature sensor) would need to be added upon sample heating but more dissipated upon cooling through a full transition cycle. However, neither the heating nor the cooling branch in Figure 6.11a shows a progressive lowering of T_c as the VO_2 NPs (hence, the Au caps) increase in size. Therefore, plasmonic heating of the VO_2 NPs by the Au caps, albeit possible in principle, is not borne out by the present data.

A measure of the intrinsic size-dependence of the phase transition that would remain unaffected by a constant temperature bias is the width of the thermal hysteresis. As mentioned before, a contiguous VO_2 film has a relatively narrow hysteresis (typically ΔT = 10–15 K) because many potent sites for heterogeneous nucleation reside in its large accessible volume, so that relatively small excursions in temperature can initiate the phase transition. On the contrary, smaller amounts of VO_2 material generally require substantial overheating and undercooling (*i.e.*, excess driving forces) to change from the monoclinic into the tetragonal phase and back, thereby exhibiting a wide thermal hysteresis. Figure 6.11b, where the square points are obtained directly from Figure 6.11a, further corroborates this trend: $\Delta T_{\text{film}} = 10.5 \pm 0.5$ K, whereas $\Delta T_{50\text{nmNPs}} = 26.5 \pm 2.5$ K. Moreover, the hysteresis width shrinks with increasing NP size (*e.g.*, $\Delta T_{150\text{nmNPs}} = 17.5 \pm 0.5$ K), as expected from the model,[5] since an increase in the probed volume per particle should result in a greater average probability that any given NP contains at least one random site capable of heterogeneously nucleating the phase transition.

Also shown in Figure 6.11b (circles) are the hysteresis widths for arrays of VO_2 NPs from the above-mentioned light-scattering experiments of Lopez *et al.*[9] The values were computed from the points in Figure 6.1c as $\Delta T_{\text{Lopez}} = T_{\text{C}} - T_{\text{G}}$. Points "C" and "G" were chosen because they mark the temperatures of maximum disorder in those NP arrays, when about half of all NPs have turned metallic during heating ("C") or semiconducting during cooling ("G") (see also Figure 4d in Reference [9]). In comparison with the present study (Figure 6.11b, squares), Lopez *et al.*'s VO_2 NPs demonstrate a stronger size-dependence both in terms of the magnitude and slope of ΔT. It may be tempting to rationalize these discrepancies as due to probing the two different components of the VO_2 phase transition—electronic (via elastic light scattering) *vs.* structural (via SERS)—but such a statement could be misleading. In hindsight, the Au caps utilized in this study likely play a dual role: above all, to greatly enhance the weak Raman signal from the VO_2 NPs, but also, possibly, to introduce new "potent defects" during the thermal anneal (step (v) in Section 6.2). The

finger-like protrusions mentioned in Section 6.2 give visual clues that the presence of the Au layer does impact the growth of the underlying VO_2 NP; in fact, doping VO_2 films with Au has been shown to reduce the width and sharpness of the hysteresis of the IR transmission.[91] Adding extrinsic defect sites to the ones mandated by the statistics of heterogeneous nucleation[5] would be expected to narrow the hysteresis width and, to some extent, obscure its dependence on particle size. Nevertheless, the present study lends further experimental support to the notion that the size-effect in the VO_2 phase transition is a statistical manifestation of a more fundamental criterion—the presence or absence of nucleating sites active at a given temperature.

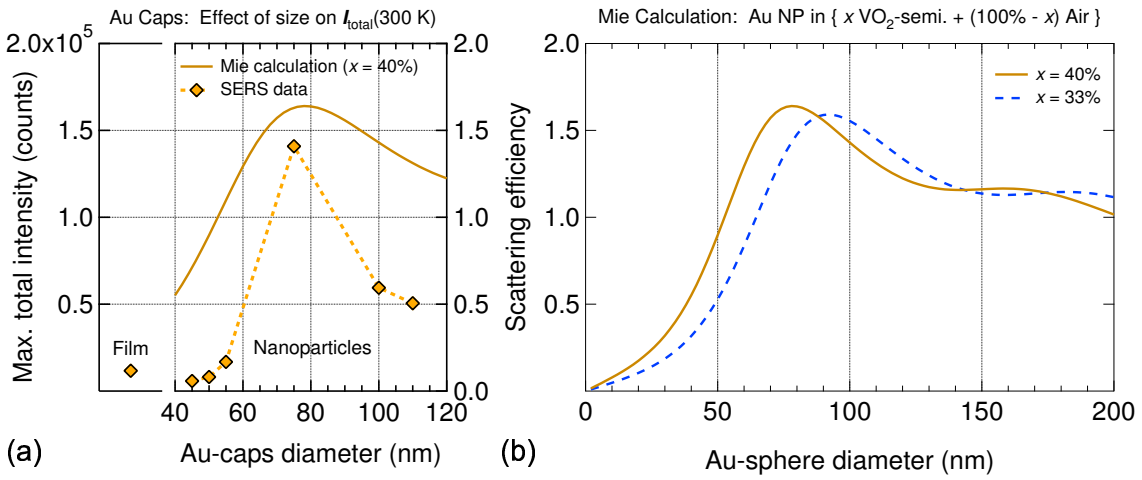

Figure 6.12: **(a)** Total SERS intensity at 300 K (from hysteresis curves in Figures 6.8, 6.9, and 6.10) as a function of size of the Au caps (right panel); dashed line is only a guide for the eye; solid line is one of the Mie calculations shown in **(b)**; the value for the Au+VO_2 film is also shown (left panel). **(b)** Mie-theory calculations (modified for absorbing host medium) of scattering efficiency as a function of particle diameter for Au sphere in composite host medium consisting of $\frac{2}{5}$ ($x = 40\%$) semiconducting-phase VO_2 and $\frac{3}{5}$ Air, compared to the calculation from Figure 6.3. The highest efficiency for $x = 40$ % occurs near $2r_{\mathrm{Au}} = 75$ nm, closely matching the largest measured SERS intensity in **(a)**.

6.3.3 Size-dependence of the SERS intensity

We now briefly return to the SERS effect, which made this study altogether possible (see Figure 6.2), and quantify its dependence on particle size. As mentioned earlier in connection with Figure 6.3, Mie theory predicts the scattering efficiency of a spherical Au NP to peak at $2r_{\mathrm{Au}} = 90$ nm when the particle resides in an effective external medium consisting of 33% VO_2 and 67% air; hence, the 90-nm VO_2 NPs capped with Au hemispheres (Figure 6.10a) were expected to exhibit the strongest enhancement of the VO_2 Raman signal. Indeed, even a cursory glance at the hysteresis maxima reveals this to be the case: cf, I_{total} at 300 K in Figures 6.8c, 6.9(b, d, f), and 6.10(b, d, f). These maxima of the total Raman intensity of the two VO_2 peaks are plotted in Figure 6.12a; the particle sizes here refer to the diameters of the Au caps, which further image analysis (*i.e.*, higher grey-level threshold) determined to be approximately 5 to 40 nm smaller than the underlying VO_2 NPs (*e.g.*, see Figure 6.10e). The strongest SERS signal therefore came from "90-nm VO_2 NPs with 75-nm Au caps atop". It turns out that the Mie calculation in Figure 6.3 requires only a relatively small parameter adjustment—40% instead of 33% VO_2 contribution—to yield a maximum in the Au-NP scattering efficiency at $2r_{\mathrm{Au}} = 75$ nm (Figure 6.12b, also overlaid on the experimental data in Figure 6.12a). This situation (40% VO_2, 60% air) corresponds to a contact angle of less than 90° between the Au caps and the underlying VO_2 layer. Considering the simplifications employed in this calculation, such as spherical Au particles and a weighted average for the optical constants of the host medium, the qualitative agreement between the size-dependence of the measured SERS signal and the size-dependence of the calculated scattering efficiency seems quite encouraging (Figure 6.12a).

6.4 Summary and outlook

We reported the first experimental application of surface-enhanced Raman scattering (SERS) to the study of the phase transition of VO_2. The electromagnetic enhancement of the VO_2 Raman signal, caused by the plasmonic properties of Au particles, was instrumental

to this experiment, since no Raman signal could be obtained from bare VO_2 NPs of sizes less than 125 nm. The structures fabricated on a Si substrate were: **(i)** VO_2 NPs of different diameters (50 to 150 nm), arranged in regular arrays of nominally identical NPs, with each VO_2 NP capped with a somewhat smaller Au particle (45 to 110 nm); and **(ii)** a contiguous VO_2 film covered with disconnected Au islands. On comparing NPs to film, we found that the film required a smaller "driving force" to complete the phase transformation, as evidenced by its much narrower thermal hysteresis. We also observed the trend expected from a model of heterogeneous nucleation of the VO_2 phase transition,[5] namely that the 50-nm VO_2 NPs produced the widest thermal hysteresis (Figure 6.11b), since the smallest volume should have the least statistical likelihood of harboring a potent site for nucleating the phase transition. The size-effect proved less pronounced for the Au+VO_2 NPs studied here than for the bare-VO_2 NPs in Lopez *et al.*'s light-scattering experiment.[9] We offer a heuristic explanation: During high-temperature annealing, the Au metal may contribute extrinsic defects to the VO_2 NPs, thus masking the correlation between size (scarcity of nucleation sites) and hysteresis width (driving force needed to activate latent nucleation sites). Nevertheless, another size effect was clearly evident: The measured SERS intensity scaled according to NP size, peaking for the 75-nm-Au+90-nm-VO_2 NPs (Figure 6.12a), in good agreement with Mie-theory predictions for the scattering efficiency of a Au sphere surrounded by a mixture of VO_2 and air (Figure 6.12b).

The experiment described here can undoubtedly improve the throughput of a confocal Raman mapping measurement such as that proposed at the end of Chapter V: constructing many single-NP Raman hystereses in order to look for a statistical correlation between hysteresis width and VO_2 NP morphology. Ironically, the presence of the Au caps, so crucial in the SERS process, also constitutes the chief drawback of this method, for it remains unknown as to what extent the Au material alters the phase transition properties of VO_2 during the thermal anneal of a Au+VO_2 hybrid nanostructure.

REFERENCES

[1] C. Kübler, H. Ehrke, R. Huber, R. Lopez, A. Halabica, R. F. Haglund, and A. Leitenstorfer, *Physical Review Letters* **99**, 116401 (2007).

[2] M. M. Qazilbash, M. Brehm, B. G. Chae, P. C. Ho, G. O. Andreev, B. J. Kim, S. J. Yun, A. V. Balatsky, M. B. Maple, F. Keilmann, H. T. Kim, and D. N. Basov, *Science* **318**, 1750 (2007).

[3] P. Baum, D. S. Yang, and A. H. Zewail, *Science* **318**, 788 (2007).

[4] A. Sharoni, J. G. Ramírez, and I. K. Schuller, *Physical Review Letters* **101**, 026404 (2008).

[5] R. Lopez, T. E. Haynes, L. A. Boatner, L. C. Feldman, and R. F. Haglund, *Physical Review B* **65**, 224113 (2002).

[6] T. W. Ebbesen, H. J. Lezec, H. F. Ghaemi, T. Thio, and P. A. Wolff, *Nature* **391**, 667 (1998).

[7] T. J. Kim, T. Thio, T. W. Ebbesen, D. E. Grupp, and H. J. Lezec, *Optics Letters* **24**, 256 (1999).

[8] J. Dintinger, A. Degiron, and T. W. Ebbesen, *MRS Bulletin* **30**, 381 (2005).

[9] R. Lopez, L. C. Feldman, and R. F. Haglund, *Physical Review Letters* **93**, 177403 (2004).

[10] C. X. Wang and G. W. Yang, *Materials Science & Engineering R: Reports* **49**, 157 (2005).

[11] J. G. Lee and H. Mori, *Physical Review Letters* **93**, 235501 (2004).

[12] K. K. Nanda, A. Maisels, F. E. Kruis, H. Fissan, and S. Stappert, *Physical Review Letters* **91**, 106102 (2003).

[13] T. Shibata, B. A. Bunker, Z. Y. Zhang, D. Meisel, C. F. Vardeman, and J. D. Gezelter, *Journal of the American Chemical Society* **124**, 11989 (2002).

[14] T. Shinohara, T. Sato, and T. Taniyama, *Physical Review Letters* **91**, 197201 (2003).

[15] H. J. Mamin, R. Budakian, B. W. Chui, and D. Rugar, *Physical Review Letters* **91**, 207604 (2003).

[16] K. Dick, T. Dhanasekaran, Z. Zhang, and D. Meisel, *Journal of the American Chemical Society* **124**, 2312 (2002).

[17] R. A. Masumura, P. M. Hazzledine, and C. S. Pande, *Acta Materialia* **46**, 4527 (1998).

[18] D. Katz, T. Wizansky, O. Millo, E. Rothenberg, T. Mokari, and U. Banin, *Physical Review Letters* **89**, 199901 (2002).

[19] J. T. Lau, A. Fohlisch, R. Nietubyc, M. Reif, and W. Wurth, *Physical Review Letters* **89**, 057201 (2002).

[20] C. Voisin, D. Christofilos, N. D. Fatti, F. Vallee, B. Prevel, E. Cottancin, J. Lerme, M. Pellarin, and M. Broyer, *Physical Review Letters* **85**, 2200 (2000).

[21] F. J. Morin, *Physical Review Letters* **3**, 34 (1959).

[22] J. B. Goodenough, *Journal of Solid State Chemistry* **3**, 490 (1971).

[23] M. Imada, A. Fujimori, and Y. Tokura, *Reviews of Modern Physics* **70**, 1039 (1998).

[24] P. A. Cox, *Transition metal oxides: An introduction to their electronic structure and properties*, The International Series of Monographs on Chemistry, Clarendon Press; Oxford University Press, Oxford New York, 1992.

[25] A. Zylbersztejn and N. F. Mott, *Physical Review B* **11**, 4383 (1975).

[26] D. Paquet and P. L. Hugon, *Physical Review B* **22**, 5284 (1980).

[27] R. M. Wentzcovitch, W. W. Schulz, and P. B. Allen, *Physical Review Letters* **73**, 3043 (1994).

[28] T. M. Rice, H. Launois, and J. P. Pouget, *Physical Review Letters* **73**, 3042 (1994).

[29] R. M. Wentzcovitch, W. W. Schulz, and P. B. Allen, *Physical Review Letters* **72**, 3389 (1994).

[30] S. Biermann, A. Poteryaev, A. I. Lichtenstein, and A. Georges, *Physical Review Letters* **94**, 026404 (2005).

[31] A. Cavalleri, T. Dekorsy, H. H. W. Chong, J. C. Kieffer, and R. W. Schoenlein, *Physical Review B* **70**, 161102 (2004).

[32] H. T. Kim, Y. W. Lee, B. J. Kim, B. G. Chae, S. J. Yun, K. Y. Kang, K. J. Han, K. J. Yee, and Y. S. Lim, *Physical Review Letters* **97**, 266401 (2006).

[33] A. Cavalleri, M. Rini, and R. W. Schoenlein, *Journal of the Physical Society of Japan* **75**, 011004 (2006).

[34] V. S. Vikhnin, S. Lysenko, A. Rua, F. Fernandez, and H. Liu, *Solid State Communications* **137**, 615 (2006).

[35] S. Lysenko, A. J. Rua, V. Vikhnin, J. Jimenez, F. Fernandez, and H. Liu, *Applied Surface Science* **252**, 5512 (2006).

[36] M. S. Grinolds, V. A. Lobastov, J. Weissenrieder, and A. H. Zewail, *Proceedings of the National Academy of Sciences of the United States of America* **103**, 18427 (2006).

[37] I. Yamashita, H. Kawaji, T. Atake, Y. Kuroiwa, and A. Sawada, *Physical Review B* **68**, 092104 (2003).

[38] A. S. Shirinyan and M. Wautelet, *Nanotechnology* **15**, 1720 (2004).

[39] G. F. Goya, M. Veith, R. Rapalavicuite, H. Shen, and S. Mathur, *Applied Physics A: Materials Science & Processing* **80**, 1523 (2005).

[40] K. Jacobs, J. Wickham, and A. P. Alivisatos, *Journal of Physical Chemistry B* **106**, 3759 (2002).

[41] D. Zaziski, S. Prilliman, E. C. Scher, M. Casula, J. Wickham, S. M. Clark, and A. P. Alivisatos, *Nano Letters* **4**, 943 (2004).

[42] Q. Xu, I. D. Sharp, C. W. Yuan, D. O. Yi, C. Y. Liao, A. M. Glaeser, A. M. Minor, J. W. Beeman, M. C. Ridgway, P. Kluth, I. Ager, J. W., D. C. Chrzan, and E. E. Haller, *Physical Review Letters* **97**, 155701 (2006).

[43] R. E. Cech and D. Turnbull, *Journal of Metals* , 124 (1956).

[44] I. W. Chen, Y. H. Chiao, and K. Tsuzaki, *Acta Metallurgica* **33**, 1847 (1985).

[45] J. Y. Suh, R. Lopez, L. C. Feldman, and R. F. Haglund, *Journal of Applied Physics* **96**, 1209 (2004).

[46] D. Brassard, S. Fourmaux, M. Jean-Jacques, J. C. Kieffer, and M. A. El Khakani, *Applied Physics Letters* **87**, 051910 (2005).

[47] R. A. Aliev, V. N. Andreev, V. M. Kapralova, V. A. Klimov, A. I. Sobolev, and E. B. Shadrin, *Physics of the Solid State* **48**, 929 (2006).

[48] J. Rozen, R. Lopez, R. F. Haglund, and L. C. Feldman, *Applied Physics Letters* **88**, 081902 (2006).

[49] K. Nagashima, T. Yanagida, H. Tanaka, and T. Kawai, *Journal of Applied Physics* **101**, 026103 (2007).

[50] R. Lopez, L. A. Boatner, T. E. Haynes, R. F. Haglund, and L. C. Feldman, *Applied Physics Letters* **79**, 3161 (2001).

[51] R. Lopez, L. A. Boatner, T. E. Haynes, L. C. Feldman, and R. F. Haglund, *Journal of Applied Physics* **92**, 4031 (2002).

[52] R. Lopez, T. E. Haynes, L. A. Boatner, L. C. Feldman, and R. F. Haglund, *Optics Letters* **27**, 1327 (2002).

[53] R. Lopez, J. Y. Suh, L. C. Feldman, and R. F. Haglund, *Symposium Proceedings of the Materials Research Society* **820**, R1.5 (2004).

[54] M. Rini, A. Cavalleri, R. W. Schoenlein, R. Lopez, L. C. Feldman, R. F. Haglund, L. A. Boatner, and T. E. Haynes, *Optics Letters* **30**, 558 (2005).

[55] V. Eyert, *Annalen der Physik* **11**, 650 (2002).

[56] M. M. Qazilbash, K. S. Burch, D. Whisler, D. Shrekenhamer, B. G. Chae, H. T. Kim, and D. N. Basov, *Physical Review B* **74**, 205118 (2006).

[57] H. W. Verleur, A. S. Barker, and C. N. Berglund, *Physical Review* **172**, 788 (1968).

[58] S. Shin, S. Suga, M. Taniguchi, M. Fujisawa, H. Kanzaki, A. Fujimori, H. Daimon, Y. Ueda, K. Kosuge, and S. Kachi, *Physical Review B* **41**, 4993 (1990).

[59] M. M. Qazilbash, A. A. Schafgans, K. S. Burch, S. J. Yun, B. G. Chae, B. J. Kim, H. T. Kim, and D. N. Basov, *Physical Review B* **77**, 115121 (2008).

[60] S. Lysenko, V. Vikhnin, F. Fernandez, A. Rua, and H. Liu, *Physical Review B* **75**, 075109 (2007).

[61] C. Kittel, *Introduction to solid state physics*, Wiley, New York, 7th edition, 1996.

[62] J. Spalek, Superconductivity mechanisms, in *Encyclopedia of Modern Physics*, edited by R. A. Meyers and S. N. Shore, pp. 679–716, Academic Press, San Diego, 1990.

[63] T. M. Rice and D. B. McWhan, *IBM Journal of Research and Development* **14**, 251 (1970).

[64] N. F. Mott, *Reviews of Modern Physics* **40**, 677 (1968).

[65] J. Hubbard, *Proceedings of the Royal Society of London. Series A, Mathematical and Physical Sciences* **276**, 238 (1963).

[66] A. I. Buzdin and L. N. Bulayevskii, *Uspekhi Fizicheskikh Nauk* **131**, 495 (1980).

[67] J. M. Tomczak and S. Biermann, *Journal of Physics: Condensed Matter* **19**, 365206 (2007).

[68] M. W. Haverkort, Z. Hu, A. Tanaka, W. Reichelt, S. V. Streltsov, M. A. Korotin, V. I. Anisimov, H. H. Hsieh, H. J. Lin, C. T. Chen, D. I. Khomskii, and L. H. Tjeng, *Physical Review Letters* **95**, 196404 (2005).

[69] C. Kübler, H. Ehrke, A. Leitenstorfer, R. Lopez, A. Halabica, and R. F. Haglund, Ultrafast Conductivity and Lattice Dynamics of Insulator-Metal Phase Transition in VO2 Studied via Multi-Terahertz Spectroscopy, in *Joint 31st Int'l Conference on Infrared and Millimeter Waves and 14th Int'l Conference on Terahertz Electronics (IRMMW-THz'06)*, Shanghai, China, 2006.

[70] C. N. R. Rao and K. J. Rao, *Phase transitions in solids: an approach to the study of the chemistry and physics of solids*, McGraw-Hill, New York, 1978.

[71] C. N. Berglund and H. J. Guggenheim, *Physical Review* **185**, 1022 (1969).

[72] J. Ortín, A. Planes, and L. Delaey, Hysteresis in Shape-Memory Materials, in *The Science of Hysteresis*, edited by G. Bertotti and I. D. Mayergoyz, volume 3, pp. 467–553, Elsevier, London, 2005.

[73] L. Delaey, Diffusionless Transformations, in *Phase Transformations in Materials*, edited by G. Kostorz, pp. 583–654, Wiley-VCH, Weinheim; New York; Chichester, new edition, 2001.

[74] P. C. Clapp, *Journal de Physique IV* **5**, 11 (1995).

[75] I. A. Khakhaev, F. A. Chudnovskii, and E. B. Shadrin, *Fizika Tverdogo Tela* **36**, 1643 (1994).

[76] H. S. Choi, J. S. Ahn, J. H. Jung, T. W. Noh, and D. H. Kim, *Physical Review B* **54**, 4621 (1996).

[77] F. J. Perez-Reche, E. Vives, L. Manosa, and A. Planes, *Physical Review Letters* **8719**, 195701 (2001).

[78] D. Maurer, A. Leue, R. Heichele, and V. Müller, *Physical Review B* **60**, 13249 (1999).

[79] J. Narayan and V. M. Bhosle, *Journal of Applied Physics* **100**, 103524 (2006).

[80] L. A. L. de Almeida, G. S. Deep, A. M. N. Lima, H. F. Neff, and R. C. S. Freire, *Ieee Transactions on Instrumentation and Measurement* **50**, 1030 (2001).

[81] V. A. Klimov, I. O. Timofeeva, S. D. Khanin, E. B. Shadrin, A. V. Ilinskii, and F. Silva-Andrade, *Technical Physics* **47**, 1134 (2002).

[82] R. A. Aliev and V. A. Klimov, *Physics of the Solid State* **46**, 532 (2004).

[83] R. A. Aliev, V. N. Andreev, V. A. Klimov, V. M. Lebedev, S. E. Nikitin, E. I. Terukov, and E. B. Shadrin, *Technical Physics* **50**, 754 (2005).

[84] W. Haidinger and D. Gross, *Thin Solid Films* **12**, 433 (1972).

[85] Y. Muraoka and Z. Hiroi, *Applied Physics Letters* **80**, 583 (2002).

[86] G. Xu, P. Jin, M. Tazawa, and K. Yoshimura, *Applied Surface Science* **244**, 449 (2005).

[87] E. Kusano and J. A. Theil, *Journal of Vacuum Science & Technology A: Vacuum Surfaces and Films* **7**, 1314 (1989).

[88] V. A. Klimov, I. O. Timofeeva, S. D. Khanin, E. B. Shadrin, A. V. Il'inskii, and F. Silva-Andrade, *Semiconductors* **37**, 370 (2003).

[89] F. Beteille and J. Livage, *Journal of Sol-Gel Science and Technology* **13**, 915 (1998).

[90] W. Burkhardt, T. Christmann, B. K. Meyer, W. Niessner, D. Schalch, and A. Scharmann, *Thin Solid Films* **345**, 229 (1999).

[91] E. Cavanna, J. P. Segaud, and J. Livage, *Materials Research Bulletin* **34**, 167 (1999).

[92] F. C. Case, *Journal of Vacuum Science & Technology A: Vacuum Surfaces and Films* **2**, 1509 (1984).

[93] F. C. Case, *Journal of Vacuum Science & Technology A: Vacuum Surfaces and Films* **7**, 1194 (1989).

[94] A. Leone, A. M. Trione, and F. Junga, *IEEE Transactions on Nuclear Science* **37**, 1739 (1990).

[95] P. Jin, S. Nakao, and S. Tanemura, *Nuclear Instruments & Methods in Physics B: Beam Interactions with Materials & Atoms* **141**, 419 (1998).

[96] L. B. Lin, T. C. Lu, Q. Liu, Y. Lu, and X. D. Feng, *Surface & Coatings Technology* **158**, 530 (2002).

[97] F. Beteille, L. Mazerolles, and J. Livage, *Materials Research Bulletin* **34**, 2177 (1999).

[98] C. Petit, J. M. Frigerio, and M. Goldmann, *Journal of Physics-Condensed Matter* **11**, 3259 (1999).

[99] K. Y. Tsai, T. S. Chin, H. P. D. Shieh, and C. H. Ma, *Journal of Materials Research* **19**, 2306 (2004).

[100] I. Karakurt, J. Boneberg, P. Leiderer, R. Lopez, A. Halabica, and R. F. Haglund, *Applied Physics Letters* **91**, 091907 (2007).

[101] J. E. Mahan, *Physical vapor deposition of thin films*, Wiley, New York; Chichester, 2000.

[102] O. Svelto, S. Longhi, G. D. Valle, S. Kück, G. Huber, M. Pollnau, and H. Hillmer etc., Lasers and Coherent Light Sources, in *Springer Handbook of Lasers and Optics*, edited by F. Träger, pp. 583–936, Springer, New York, 2007.

[103] N. D. Bassim, P. K. Schenck, E. U. Donev, E. J. Heilweil, E. Cockayne, M. L. Green, and L. C. Feldman, *Applied Surface Science* **254**, 785 (2007).

[104] C. A. Volkert and A. M. Minor, *MRS Bulletin* **32**, 389 (2007).

[105] P. Rai-Choudhury, *Handbook of Microlithography, Micromachining, and Microfabrication*, volume 1, SPIE Optical Engineering Press; Institution of Electrical Engineers, Bellingham, Wash., USA London, UK, 1997.

[106] T. L. Alford, L. C. Feldman, and J. W. Mayer, *Fundamentals of nanoscale film analysis*, Springer, New York; London, 2007.

[107] M. Mayer, *SIMNRA (ver. 5.02)*, http://www.ipp.mpg.de/∼mam, 2004.

[108] K. Iizuka, *Elements of photonics*, Wiley Series in Pure and Applied Optics, Wiley, New York, 2002.

[109] WITec, *AlphaSNOM Manual*, WITec Wissenschaftliche Instrumente und Technologie GmbH, 2002.

[110] M. Fox, *Optical properties of solids*, Oxford Master Series in Condensed Matter Physics, Oxford University Press, Oxford; New York, 2001.

[111] G. Brooker, *Modern classical optics*, Oxford University Press, Oxford, 2003.

[112] L. Novotny and B. Hecht, *Principles of Nano-Optics*, Cambridge University Press, 2006.

[113] S. A. Maier and H. A. Atwater, *Journal of Applied Physics* **98**, 011101 (2005).

[114] U. Kreibig, M. Gartz, A. Hilger, and H. Hovel, *Optical investigations of surfaces and interfaces of metal clusters*, volume 4, JAI Press, Inc., Stanford, 1998.

[115] K. L. Kelly, E. Coronado, L. L. Zhao, and G. C. Schatz, *Journal of Physical Chemistry B* **107**, 668 (2003).

[116] J. D. Jackson, *Classical electrodynamics*, Wiley, New York, 3rd edition, 1999.

[117] M. L. Sandrock and C. A. Foss, *Journal of Physical Chemistry B* **103**, 11398 (1999).

[118] G. Mie, *Annalen der Physik* **25**, 377 (1908).

[119] I. W. Sudiarta and P. Chylek, *Journal of the Optical Society of America A* **18**, 1275 (2001).

[120] H. C. van de Hulst, *Light Scattering by Small Particles*, Dover Publications, Inc., New York, 1981.

[121] M. B. Cortie, A. Dowd, N. Harris, and M. J. Ford, *Physical Review B* **75**, 113405 (2007).

[122] L. R. Hirsch, R. J. Stafford, J. A. Bankson, S. R. Sershen, B. Rivera, R. E. Price, J. D. Hazle, N. J. Halas, and J. L. West, *Proceedings of the National Academy of Sciences of the United States of America* **100**, 13549 (2003).

[123] J. M. Brockman, B. P. Nelson, and R. M. Corn, *Annual Review of Physical Chemistry* **51**, 41 (2000).

[124] E. U. Donev, J. Y. Suh, F. Villegas, R. Lopez, R. F. Haglund, and L. C. Feldman, *Physical Review B* **73**, 201401 (2006).

[125] J. Y. Suh, E. U. Donev, R. Lopez, L. C. Feldman, and R. F. Haglund, *Applied Physics Letters* **88**, 133115 (2006).

[126] A. Bianconi, S. Stizza, and R. Bernardini, *Physical Review B* **24**, 4406 (1981).

[127] Y. N. Xia and N. J. Halas, *MRS Bulletin* **30**, 338 (2005).

[128] G. Xu, Y. Chen, M. Tazawa, and P. Jin, *Journal of Physical Chemistry B* **110**, 2051 (2006).

[129] E. A. Coronado and G. C. Schatz, *Journal of Chemical Physics* **119**, 3926 (2003).

[130] M. Maaza, O. Nemraoui, C. Sella, A. C. Beye, and B. Baruch-Barak, *Optics Communications* **254**, 188 (2005).

[131] W. Rechberger, A. Hohenau, A. Leitner, J. R. Krenn, B. Lamprecht, and F. R. Aussenegg, *Optics Communications* **220**, 137 (2003).

[132] J. Y. Suh, E. U. Donev, D. W. Ferrara, K. A. Tetz, L. C. Feldman, and R. F. Haglund, *Journal of Optics A: Pure and Applied Optics* , 055202 (2008).

[133] M. D. McMahon, R. Lopez, R. F. Haglund, E. A. Ray, and P. H. Bunton, *Physical Review B* **73**, 041401 (2006).

[134] S. Wang, D. F. P. Pile, C. Sun, and X. Zhang, *Nano Letters* **7**, 1076 (2007).

[135] C. A. Foss, G. L. Hornyak, J. A. Stockert, and C. R. Martin, *Journal of Physical Chemistry* **98**, 2963 (1994).

[136] J. Grand, P. M. Adam, A. S. Grimault, A. Vial, M. L. De la Chapelle, J. L. Bijeon, S. Kostcheev, and P. Royer, *Plasmonics* **1**, 135 (2006).

[137] K. H. Su, Q. H. Wei, X. Zhang, J. J. Mock, D. R. Smith, and S. Schultz, *Nano Letters* **3**, 1087 (2003).

[138] T. R. Jensen, M. L. Duval, K. L. Kelly, A. A. Lazarides, G. C. Schatz, and R. P. Van Duyne, *Journal of Physical Chemistry B* **103**, 9846 (1999).

[139] J. J. Mock, D. R. Smith, and S. Schultz, *Nano Letters* **3**, 485 (2003).

[140] P. B. Johnson and R. W. Christy, *Physical Review B* **6**, 4370 (1972).

[141] S. Link and M. A. El-Sayed, *Journal of Physical Chemistry B* **103**, 4212 (1999).

[142] H. Bethe, *Physical Review* **66**, 163 (1944).

[143] C. J. Bouwkamp, *IEEE Transactions on Antennas and Propagation* **AP18**, 152 (1970).

[144] H. Liu and P. Lalanne, *Nature* **452**, 728 (2008).

[145] C. Liu, V. Kamaev, and Z. V. Vardeny, *Applied Physics Letters* **86**, 143501 (2005).

[146] A. Krishnan, T. Thio, T. J. Kima, H. J. Lezec, T. W. Ebbesen, P. A. Wolff, J. Pendry, L. Martin-Moreno, and F. J. Garcia-Vidal, *Optics Communications* **200**, 1 (2001).

[147] E. Hendry, M. J. Lockyear, J. Gómez-Rivas, L. Kuipers, and M. Bonn, *Physical Review B* **75**, 235305 (2007).

[148] E. U. Donev, J. Y. Suh, R. Lopez, L. C. Feldman, and R. F. Haglund, *Advances in OptoElectronics* , 739135 (2008).

[149] S. G. Tikhodeev, A. L. Yablonskii, E. A. Muljarov, N. A. Gippius, and T. Ishihara, *Physical Review B* **66**, 045102 (2002).

[150] A. Roberts, *Journal of the Optical Society of America A: Optics Image Science and Vision* **4**, 1970 (1987).

[151] A. Liebsch, *Physical Review Letters* **71**, 145 (1993).

[152] W. L. Barnes, *Journal of Optics A: Pure and Applied Optics* **8**, S87 (2006).

[153] H. Raether, *Springer Tracts in Modern Physics* **111**, 1 (1988).

[154] W. L. Barnes, A. Dereux, and T. W. Ebbesen, *Nature* **424**, 824 (2003).

[155] A. V. Zayats, L. Salomon, and F. de Fornel, *Journal of Microscopy* **210**, 344 (2003).

[156] H. F. Ghaemi, T. Thio, D. E. Grupp, T. W. Ebbesen, and H. J. Lezec, *Physical Review B* **58**, 6779 (1998).

[157] D. S. Kim, S. C. Hohng, V. Malyarchuk, Y. C. Yoon, Y. H. Ahn, K. J. Yee, J. W. Park, J. Kim, Q. H. Park, and C. Lienau, *Physical Review Letters* **91**, 143901 (2003).

[158] P. Lalanne, J. C. Rodier, and J. P. Hugonin, *Journal of Optics A: Pure and Applied Optics* **7**, 422 (2005).

[159] E. Popov, M. Neviere, S. Enoch, and R. Reinisch, *Physical Review B* **62**, 16100 (2000).

[160] S. Enoch, E. Popov, M. Neviere, and R. Reinisch, *Journal of Optics A: Pure and Applied Optics* **4**, S83 (2002).

[161] T. Thio, H. F. Ghaemi, H. J. Lezec, P. A. Wolff, and T. W. Ebbesen, *Journal of the Optical Society of America B: Optical Physics* **16**, 1743 (1999).

[162] L. Martin-Moreno, F. J. Garcia-Vidal, H. J. Lezec, K. M. Pellerin, T. Thio, J. B. Pendry, and T. W. Ebbesen, *Physical Review Letters* **86**, 1114 (2001).

[163] S. A. Darmanyan and A. V. Zayats, *Physical Review B* **67**, 035424 (2003).

[164] W. L. Barnes, W. A. Murray, J. Dintinger, E. Devaux, and T. W. Ebbesen, *Physical Review Letters* **92**, 107401 (2004).

[165] H. J. Lezec and T. Thio, *Optics Express* **12**, 3629 (2004).

[166] G. Gay, O. Alloschery, B. V. De Lesegno, C. O'Dwyer, J. Weiner, and H. J. Lezec, *Nature Physics* **2**, 262 (2006).

[167] G. Gay, O. Alloschery, B. V. de Lesegno, J. Weiner, and H. J. Lezec, *Physical Review Letters* **96**, 213901 (2006).

[168] G. Gay, O. Alloschery, J. Weiner, H. J. Lezec, C. O'Dwyer, M. Sukharev, and T. Seideman, *Physical Review E* **75**, 016612 (2007).

[169] P. Lalanne and J. P. Hugonin, *Nature Physics* **2**, 551 (2006).

[170] F. Kalkum, G. Gay, O. Alloschery, J. Weiner, H. J. Lezec, Y. Xie, and M. Mansuripur, *Optics Express* **15**, 2613 (2007).

[171] G. Gay, O. Alloschery, J. Weiner, H. J. Lezec, C. O'Dwyer, M. Sukharev, and T. Seideman, *Nature Physics* **2**, 792 (2006).

[172] F. J. Garcia-Vidal, S. G. Rodrigo, and L. Martin-Moreno, *Nature Physics* **2**, 790 (2006).

[173] P. Lalanne, J. P. Hugonin, M. Besbes, and P. Bienstman, *Nature Physics* **2**, 792 (2006).

[174] J. Weiner and H. J. Lezec, *Nature Physics* **2**, 791 (2006).

[175] A. Degiron and T. W. Ebbesen, *Journal of Optics A: Pure and Applied Optics* **7**, S90 (2005).

[176] C. Genet, M. P. van Exter, and J. P. Woerdman, *Optics Communications* **225**, 331 (2003).

[177] M. Sarrazin and J. P. Vigneron, *Physical Review E* **68**, 016603 (2003).

[178] M. Sarrazin, J. P. Vigneron, and J. M. Vigoureux, *Physical Review B* **67**, 085415 (2003).

[179] A. Degiron, H. J. Lezec, W. L. Barnes, and T. W. Ebbesen, *Applied Physics Letters* **81**, 4327 (2002).

[180] K. L. van der Molen, F. B. Segerink, N. F. van Hulst, and L. Kuipers, *Applied Physics Letters* **85**, 4316 (2004).

[181] A. Hessel and A. A. Oliner, *Applied Optics* **4**, 1275 (1965).

[182] F. J. Garcia de Abajo, *Reviews of Modern Physics* **79**, 1267 (2007).

[183] J. E. Stewart and W. S. Gallaway, *Applied Optics* **1**, 421 (1962).

[184] E. D. Palik, *Handbook of optical constants of solids*, Academic Press Handbook Series, Academic Press, Orlando, 1985.

[185] W. Bogaerts, P. Bienstman, D. Taillaert, R. Baets, and D. De Zutter, *IEEE Photonics Technology Letters* **13**, 565 (2001).

[186] A. Degiron, H. J. Lezec, N. Yamamoto, and T. W. Ebbesen, *Optics Communications* **239**, 61 (2004).

[187] A. Cavalleri, C. Tóth, C. W. Siders, J. A. Squier, F. Ráksi, P. Forget, and J. C. Kieffer, *Physical Review Letters* **87**, 237401 (2001).

[188] M. F. Becker, A. B. Buckman, R. M. Walser, T. Lepine, P. Georges, and A. Brun, *Applied Physics Letters* **65**, 1507 (1994).

[189] M. F. Becker, A. B. Buckman, R. M. Walser, T. Lepine, P. Georges, and A. Brun, *Journal of Applied Physics* **79**, 2404 (1996).

[190] K. C. Kam and A. K. Cheetham, *Materials Research Bulletin* **41**, 1015 (2006).

[191] J. Park, I. H. Oh, E. Lee, K. W. Lee, C. E. Lee, K. Song, and Y. J. Kim, *Applied Physics Letters* **91**, 153112 (2007).

[192] F. Guinneton, L. Sauques, J. C. Valmalette, F. Cros, and J. R. Gavarri, *Journal of Physics and Chemistry of Solids* **62**, 1229 (2001).

[193] S. Q. Xu, H. P. Ma, S. X. Dai, and Z. H. Jiang, *Journal of Materials Science* **39**, 489 (2004).

[194] S. A. Pauli, R. Herger, P. R. Willmott, E. U. Donev, J. Y. Suh, and R. F. Haglund, *Journal of Applied Physics* **102**, 073527 (2007).

[195] K. Hyun-Tak, C. Byung-Gyu, Y. Doo-Hyeb, K. Gyungock, K. Kwang-Yong, L. Seung-Joon, K. Kwan, and L. Yong-Sik, *Applied Physics Letters* **86**, 242101 (2005).

[196] R. Srivastava and L. L. Chase, *Physical Review Letters* **27**, 727 (1971).

[197] M. Pan, J. Liu, H. M. Zhong, S. W. Wang, Z. F. Li, X. H. Chen, and W. Lu, *Journal of Crystal Growth* **268**, 178 (2004).

[198] G. I. Petrov, V. V. Yakovlev, and J. Squier, *Applied Physics Letters* **81**, 1023 (2002).

[199] J. C. Parker, *Physical Review B* **42**, 3164 (1990).

[200] H.-T. Yuan, K.-C. Feng, X.-J. Wang, C. Li, C.-J. He, and Y.-X. Nie, *Chinese Physics* , 82 (2004).

[201] P. Schilbe, *Physica B: Condensed Matter* **316**, 600 (2002).

[202] N. N. Brandt, O. O. Brovko, A. Y. Chikishev, and O. D. Paraschuk, *Applied Spectroscopy* **60**, 288 (2006).

[203] C. H. Griffiths and H. K. Eastwood, *Journal of Applied Physics* **45**, 2201 (1974).

[204] C. L. Xu, X. Ma, X. Liu, W. Y. Qiu, and Z. X. Su, *Materials Research Bulletin* **39**, 881 (2004).

[205] D. Dragoman and M. Dragoman, *Optical characterization of solids*, Springer, Berlin; New York, 2002.

[206] R. R. Andronenko, I. N. Goncharuk, V. Y. Davydov, F. A. Chudnovskii, and E. B. Shadrin, *Physics of the Solid State* **36**, 1136 (1994).

[207] P. Schilbe and D. Maurer, *Materials Science and Engineering A: Structural Materials Properties Microstructure and Processing* **370**, 449 (2004).

[208] H. H. Richardson, Z. N. Hickman, A. O. Govorov, A. C. Thomas, W. Zhang, and M. E. Kordesch, *Nano Letters* **6**, 783 (2006).

[209] A. O. Govorov, W. Zhang, T. Skeini, H. Richardson, J. Lee, and N. A. Kotov, *Nanoscale Research Letters* **1**, 84 (2006).

[210] G. A. Thomas, D. H. Rapkine, S. A. Carter, A. J. Millis, T. F. Rosenbaum, P. Metcalf, and J. M. Honig, *Physical Review Letters* **73**, 1529 (1994).

[211] S. Yonezawa, Y. Muraoka, Y. Ueda, and Z. Hiroi, *Solid State Communications* **129**, 245 (2004).

[212] F. C. Case, *Journal of Vacuum Science & Technology A: Vacuum Surfaces and Films* **9**, 461 (1991).

[213] H. Schuler, S. Grigoriev, and S. Horn, *Materials Research Society Symposium Proceedings* **474**, 291 (1997).

[214] B. Sass, C. Tusche, W. Felsch, N. Quaas, A. Weismann, and M. Wenderoth, *Journal of Physics: Condensed Matter* **16**, 77 (2004).

[215] P. A. Metcalf, S. Guha, L. P. Gonzalez, J. O. Barnes, E. B. Slamovich, and J. M. Honig, *Thin Solid Films* **515**, 3421 (2007).

[216] D. B. McWhan and J. P. Remeika, *Physical Review B* **2**, 3734 (1970).

[217] D. B. McWhan, A. Jayaraman, J. P. Remeika, and T. M. Rice, *Physical Review Letters* **34**, 547 (1975).

[218] P. Pfalzer, G. Obermeier, M. Klemm, S. Horn, and M. L. denBoer, *Physical Review B* **73**, 144106 (2006).

[219] S. Guimond, M. Abu Haija, S. Kaya, J. Lu, J. Weissenrieder, S. Shaikhutdinov, H. Kuhlenbeck, H. J. Freund, J. Dobler, and J. Sauer, *Topics in Catalysis* **38**, 117 (2006).

[220] Y. Jiang, S. Decker, C. Mohs, and K. J. Klabunde, *Journal of Catalysis* **180**, 24 (1998).

[221] N. Pinna, M. Antonietti, and M. Niederberger, *Colloids and Surfaces A: Physicochemical and Engineering Aspects* **250**, 211 (2004).

[222] C. V. Ramana, S. Utsunomiya, R. C. Ewing, and U. Becker, *Solid State Communications* **137**, 645 (2006).

[223] Z. H. Yang, P. J. Cai, L. Y. Chen, Y. L. Gu, L. Shi, A. W. Zhao, and Y. T. Qian, *Journal of Alloys and Compounds* **420**, 229 (2006).

[224] K. F. Zhang, J. S. Guo, C. H. Tao, X. Liu, H. L. Li, and Z. X. Su, *Chinese Journal of Inorganic Chemistry* **21**, 1090 (2005).

[225] K. F. Zhang, X. Z. Sun, G. W. Lou, X. Liu, H. L. Li, and Z. X. Su, *Materials Letters* **59**, 2729 (2005).